

Boosting the Ambipolar Performance of Solution-Processable Polymer Semiconductors via Hybrid Side-Chain Engineering

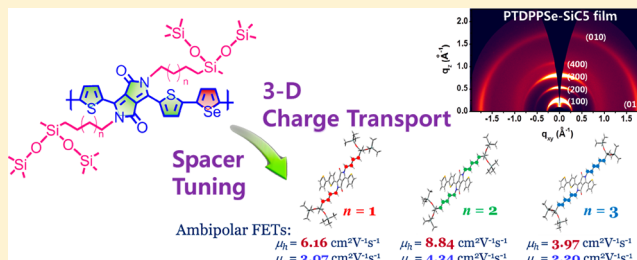
Junghoon Lee,^{†,||} A-Reum Han,^{‡,||} Hojeong Yu,[‡] Tae Joo Shin,[§] Changduk Yang,^{*,†} and Joon Hak Oh^{*,‡}

[†]Interdisciplinary School of Green Energy and [‡]School of Nano-Bioscience and Chemical Engineering, KIER-UNIST Advanced Center for Energy, Low Dimensional Carbon Materials Center, Ulsan National Institute of Science and Technology (UNIST), Ulsan 689-798, South Korea

[§]Pohang Accelerator Laboratory, Pohang University of Science and Technology, Pohang, Kyungbuk 790-784, South Korea

Supporting Information

ABSTRACT: Ambipolar polymer semiconductors are highly suited for use in flexible, printable, and large-area electronics as they exhibit both *n*-type (electron-transporting) and *p*-type (hole-transporting) operations within a single layer. This allows for cost-effective fabrication of complementary circuits with high noise immunity and operational stability. Currently, the performance of ambipolar polymer semiconductors lags behind that of their unipolar counterparts. Here, we report on the side-chain engineering of conjugated, alternating electron donor–acceptor (D–A) polymers using diketopyrrolopyrrole-selenophene copolymers with hybrid siloxane-solubilizing groups (PTDPPSe-Si) to enhance ambipolar performance. The alkyl spacer length of the hybrid side chains was systematically tuned to boost ambipolar performance. The optimized three-dimensional (3-D) charge transport of PTDPPSe-Si with pentyl spacers yielded unprecedentedly high hole and electron mobilities of 8.84 and 4.34 cm² V⁻¹ s⁻¹, respectively. These results provide guidelines for the molecular design of semiconducting polymers with hybrid side chains.



INTRODUCTION

Solution-processable polymer semiconductors intrinsically boast diverse advantages including ultralow-cost fabrication, mechanical flexibility, and tunable optoelectronic properties.^{1,2} Logic circuits based on polymer semiconductors are expected to open the possibilities of ubiquitous plastic electronics including flexible displays,^{3,4} radio frequency identification (RFID) tags,⁵ and large-area sensors.⁶ Recent efforts in molecular design^{1,7} and processing architectures^{8–11} have resulted in remarkable progress in the performance of “unipolar” field-effect transistors (FETs) based on polymer semiconductors. Nonetheless, as compared to dual unipolar component systems such as bilayers¹² or bulk-heterojunction blends,^{13,14} “ambipolar” polymer semiconductors, in which both hole- and electron-transporting functions are achieved in a single active layer, are considered to be ideal candidates for simple and low-cost fabrication of organic complementary circuits^{15,16} and light-emitting field-effect transistors (LE-FETs).^{17,18} State-of-the-art ambipolar polymers exhibit hole and electron mobilities of 0.1–1.5 cm² V⁻¹ s⁻¹.^{19–21} However, the performance of ambipolar polymer semiconductors still lags behind the best performing unipolar systems.

The rational design of novel polymers is typically based on molecular orbital energetics and crystal engineering strategies that are used to effectively tune the frontier orbital energy levels and the π -orbital overlap.^{2,22,23} To date, tremendous efforts have been focused on the design of building blocks for polymer

backbones, due to the conventional belief that the band gap and energy levels are principally determined by the molecular structure of the conjugated backbone.^{19–21,24} In contrast, relatively little attention has been paid to the molecular engineering of polymer side chains. Structural modification of polymer side chains, such as alterations in length,^{2,25} shape,²⁶ position,²⁷ bulkiness,^{28,29} symmetry,³⁰ density,³¹ and chirality,³² can substantially impact intermolecular interaction and molecular packing. Inspired by the work of Bao et al. on the effectiveness of siloxane-terminated hexyl chains on the unipolar *p*-channel operation in an isoindigo-based polymer,³³ we recently obtained ambipolar charge transport with high hole (3.97 cm² V⁻¹ s⁻¹) and electron mobilities (2.20 cm² V⁻¹ s⁻¹) by introducing selenophene units into the backbone of a diketopyrrolopyrrole (DPP)-containing copolymer with siloxane-terminated hexyl chains (PTDPPSe-SiC6).³⁴ The length of the alkyl spacer chain in the siloxane-terminated side chains affects the distance between conjugated backbones and the degree of intermolecular interaction between polymer chains. Therefore, charge transport can be optimized by tailoring the length of the alkyl spacer in the hybrid side chain. In addition, the influence of alkyl chain branching positions on charge transport was very recently examined in unipolar *p*-channel³⁵ and *n*-channel polymers.³⁶

Received: April 21, 2013

Published: May 27, 2013

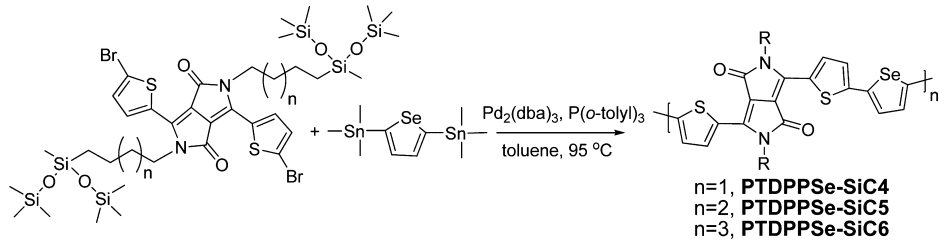


Figure 1. Synthesis and chemical structures of PTDPPSe-SiC4, PTDPPSe-SiC5, and PTDPPSe-SiC6. These copolymer structures allow systematic investigation on the siloxane-terminated side chain-dependent molecular packing and field-effect transistors performance.

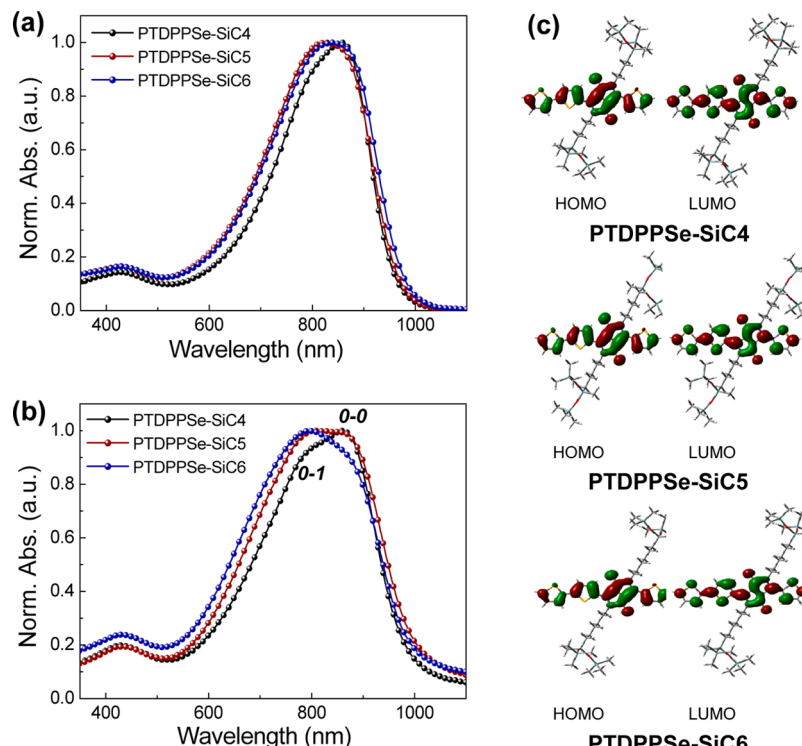


Figure 2. UV–vis absorption spectra and energy-minimized structures (B3LYP/6-31G*) of PTDPPSe-SiC4, PTDPPSe-SiC5, and PTDPPSe-SiC6. (a) Chloroform solution at room temperature. (b) Films cast from chloroform solution. (c) DFT-optimized geometries and charge-density isosurfaces for the model systems, respectively.

Herein, we present DPP-selenophene copolymers with different siloxane-terminated points, that is, butyl (PTDPPSe-SiC4) and pentyl units (PTDPPSe-SiC5), and systematically investigate the effects of hybrid side-chain spacer length on charge transport, in comparison with PTDPPSe-SiC6 and a TDPPSe-based copolymer containing alkyl chains (PTDPPSe-ref). The ambipolar performance of DPP-selenophene copolymers may be further enhanced by optimizing the branching position of hybrid side chains that controls the distance of the bulky siloxane group from the conjugated backbone. TDPPSe-Si copolymers with shorter side chains (PTDPPSe-SiC4 and PTDPPSe-SiC5) exhibited better electrical performance relative to that of PTDPPSe-SiC6. Under the same solution processing conditions, reducing the length of the siloxane-terminated side chain spacer from a hexyl to a butyl group resulted in denser microstructures and better electrical performance. Note that the solubility of PTDPPSe-SiC4 was lower than that of the analogous polymers with longer spacer groups. Therefore, homogeneous solutions of PTDPPSe-SiC4 were difficult to obtain by filtration. By utilizing a solution-shearing method that forms aligned

nanofibrillar films, unprecedentedly high hole and electron mobilities of 8.84 and $4.34 \text{ cm}^2 \text{ V}^{-1} \text{ s}^{-1}$, respectively, were obtained in homogeneous PTDPPSe-SiC5 films. To our knowledge, these are the highest hole and electron mobilities for organic- or polymer-based ambipolar FETs that have been reported to date. In addition, the electron mobility surpasses that of the highest performing polymer-based unipolar *n*-channel FETs.³⁶ Our findings demonstrate that there exists an optimal spacer length of hybrid side chains for the most effective molecular packing and highest possible charge transport. Realizing this optimum is a function of balancing polymer solubility and processing architecture. The results given herein provide guidelines for the molecular design of semiconducting polymers with siloxane-terminated solubilizing side chains.

RESULTS AND DISCUSSION

Synthetic Strategies, Synthesis, and Characterization. Two new copolymers, PTDPPSe-SiC4 and PTDPPSe-SiC5, were synthesized, and their structures are shown in Figure 1. In addition, a fresh batch of PTDPPSe-SiC6, which was

Table 1. Optical and Electrochemical Properties of PTDPPSe-SiC4, PTDPPSe-SiC5, and PTDPPSe-SiC6

polymer	$\lambda_{\max}^{\text{sol}(0-0)}$ [nm] ^a	$\lambda_{\max}^{\text{sol}(0-1)}$ [nm] ^a	$\lambda_{\max}^{\text{film}(0-0)}$ [nm]	$\lambda_{\max}^{\text{film}(0-1)}$ [nm]	E_g^{opt} [eV] ^b	E_{HOMO} [eV] ^c	E_{LUMO} [eV] ^c	E_g^{CV} [eV] ^d	$E_{\text{IP}}^{\text{UPS}}$ [eV] ^e
PTDPPSe-SiC4	857	N/A	861	791	1.25	-5.17	-3.56	1.61	4.85
PTDPPSe-SiC5	851	N/A	855	N/A	1.24	-5.10	-3.49	1.61	4.76
PTDPPSe-SiC6	855	N/A	859	793	1.23	-5.09	-3.41	1.68	4.73

^aChloroform solution. ^bDetermined from the onset of the electronic absorption spectra. ^cCyclic voltammetry determined with Fc/Fc⁺ ($E_{\text{HOMO}} = -4.80$ eV) as the external reference. ^d $E_g^{\text{CV}} = E_{\text{LUMO}} - E_{\text{HOMO}}$. ^e $E_{\text{IP}}^{\text{UPS}} = h\nu - (E_{\text{cutoff}} - E_{\text{HOMO}})$, incident photon energy ($h\nu = 21.2$ eV) for He I.

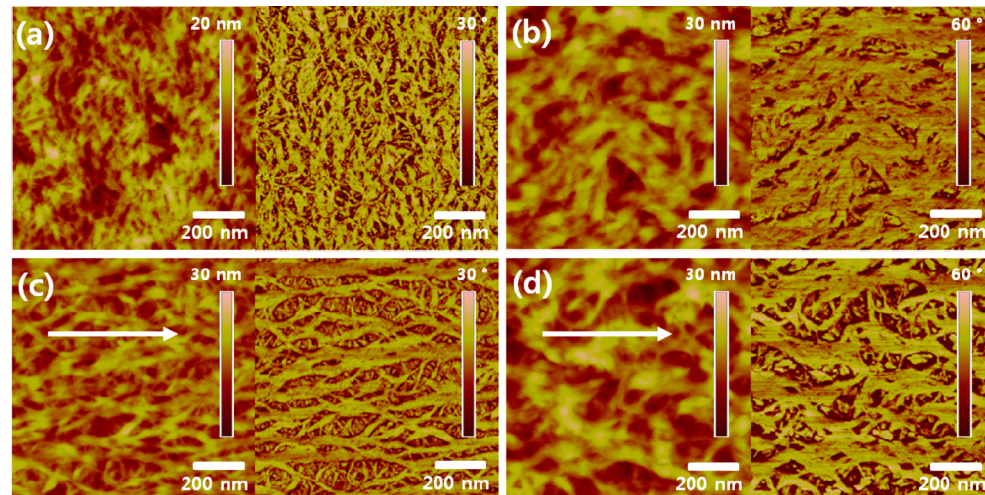


Figure 3. AFM height (left) and phase (right) images of solution-processed polymer films annealed at 220 °C. Drop-cast film of (a) PTDPPSe-SiC4 and (b) PTDPPSe-SiC5. Solution-sheared film of (c) PTDPPSe-SiC4 and (d) PTDPPSe-SiC5. The arrow indicates the direction of shearing.

investigated in a previous study,³⁴ was also prepared. This sequential series of polymers affords deeper insight into the relationship(s) between electronic properties and macromolecular structure. All intermediate materials and monomers were synthesized in their pure forms. The synthetic procedures and characterization data are described in the Supporting Information. Polymerization via Stille coupling was carried out using dibrominated TDPPs and distannylated selenophene. PTDPPSe-SiC5 and PTDPPSe-SiC6 were readily soluble in common organic solvents including THF, chloroform, and toluene. PTDPPSe-SiC4 was significantly less soluble at room temperature. Gel-permeation chromatography (GPC) at 150 °C and with 1,2,4-trichlorobenzene as the eluent revealed number-averaged molecular weights (M_n) of 25.1, 23.3, and 26.0 kDa for PTDPPSe-SiC4, PTDPPSe-SiC5, and PTDPPSe-SiC6 with polydispersities of 3.56, 3.02, and 2.79, respectively.

The absorption spectra of the three copolymers both in chloroform solution and in thin film display similar features with a broad absorption band extended from 600 to 1000 nm (Figure 2a and b), which is attributed to the intramolecular charge transfer arising from strong donor–acceptor interactions. Note that PTDPPSe-SiC4 exhibits a relatively sharp absorption peak. All of the copolymers exhibited an optical band gap of ~1.2 eV, estimated from the absorption edges of the thin films. The thin film absorption peaks are slightly broader than the peaks obtained from dissolved samples, without any obvious chromatic shift. This indicates only minimal conformational differences between the polymers dissolved in chloroform and deposited as thin films. A closer examination of the absorption features reveals that the 0–1 vibrational transition as a shorter-wavelength shoulder becomes more distinct in the PTDPPSe-SiC4 film. It is also noteworthy

that the absorption maximum of the PTDPPSe-SiC6 film is slightly blue-shifted relative to that of dissolved PTDPPSe-SiC6. This is a result of what appears to be the 0–1 vibronic profile increasing in intensity and becoming the dominant peak with a less resolved 0–0 transition. All of the photophysical data are summarized in Table 1. This observation indicates that subtle changes in the length of the siloxane-terminated side chains can greatly affect molecular packing and thin-film morphology, which in turn have a significant impact on charge transport.

The electrochemical properties of the copolymers were investigated with cyclic voltammetry (CV). All of the copolymers exhibited a stable and reversible *p*-doping/*n*-doping process in cathodic and anodic scans, respectively (Figure S1). All of these TDPPSe-Si copolymers possessed low bandgaps from 1.61 to 1.68 eV with HOMO levels from -5.09 to -5.18 eV and LUMO levels from -3.41 to -3.55 eV (Table 1). The observed differences in the HOMO and LUMO levels result from changes in film microstructure as a result of the length of the side chain. This is consistent with the aforementioned optical properties. Notably, the effect of moving the side chain termination point away from the conjugated backbone is more pronounced on the LUMO than on the HOMO. This may correlate, in part, with the degree of intermolecular interaction between the polar siloxane chains and the main backbones in the solid state. Nevertheless, molecular orbital distributions predicted by density functional theory (DFT) calculations, where each of the model systems was created with the actual siloxane-terminated side chains, showed that both the HOMO and the LUMO isosurfaces of the copolymers are extensively delocalized over the polymer backbone (Figure 2c). This is indicative of the ambipolar nature of the TDPPSe-Si copolymers.

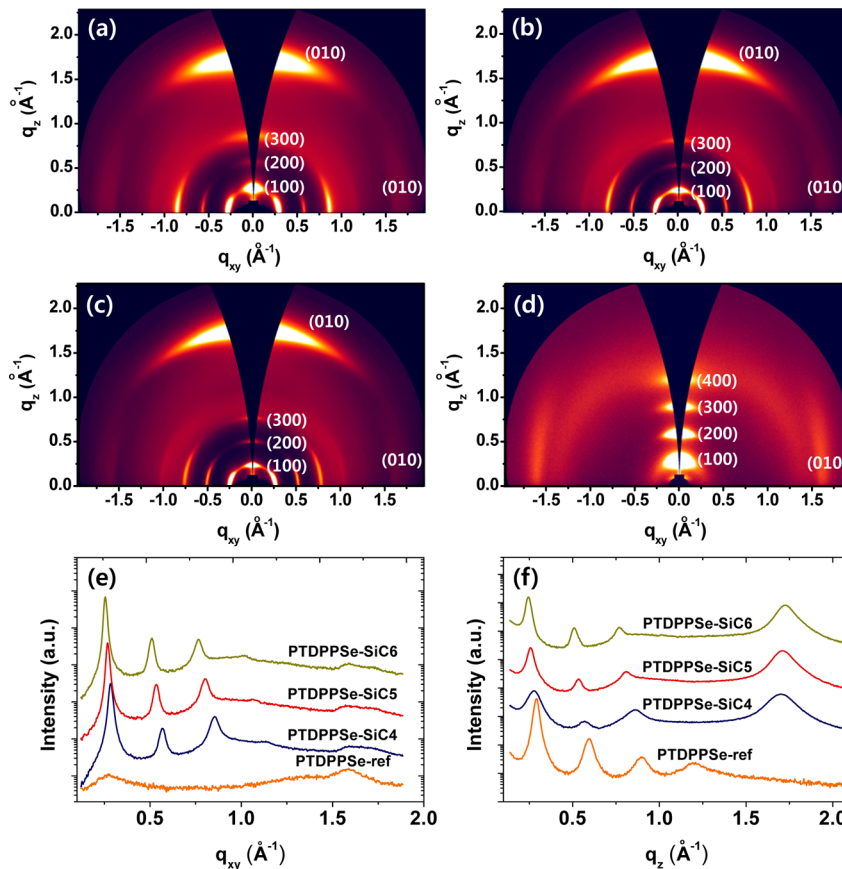


Figure 4. GIXD images of drop-cast TDPPSe-based copolymer films annealed at 220 °C: (a) PTDPPSe-SiC4, (b) PTDPPSe-SiC5, (c) PTDPPSe-SiC6, and (d) PTDPPSe-ref. The corresponding GIXD diffractogram profiles: (e) in-plane and (f) out-of-plane GIXD patterns.

The discrepancy (~0.4 eV) between the electrochemically and optically determined band gaps may be due to the exciton binding energy (0.4–1.0 eV) of conjugated polymers.^{37,38} Ionization potentials (IPs) measured by ultraviolet photo-electron spectroscopy (UPS) showed similar trends and agreed with the voltammetric results (Table 1 and Figure S2).

Thin-Film Microstructure Analyses. Tapping-mode atomic force microscopy (AFM) was performed on drop-cast and solution-sheared polymer films prepared on *n*-octadecyltrimethoxysilane (OTS)-modified SiO₂/Si substrates after thermal annealing at 220 °C (Figure 3). In the solution-shearing method, a small volume of polymer solution is placed on a substrate that has been preheated to a moderate temperature. Another plate is then pulled across the polymer solution at a controlled shearing rate, and film growth proceeds from the receding edge of the dragged plate.^{10,39}

The TDPPSe-Si copolymer films were composed of dense nanofibrillar structures with interconnected domains, implying the formation of efficient pathways for charge carrier transport. However, distinct size differences were observed between the molecular domains in PTDPPSe-SiC4 and PTDPPSe-SiC5 films. We hypothesize that these differences are closely related to the filtration process used during preparation of the polymer solutions. PTDPPSe-SiC5 films were prepared by passing the polymer solution through a syringe filter with a pore size of 0.45 μm. In contrast, because PTDPPSe-SiC4 was less soluble at room temperature, the PTDPPSe-SiC4 films were prepared from an as-dissolved solution without filtration. Therefore, aggregates of PTDPPSe-SiC4 may have been available to act as nucleation sites, resulting in an increased nuclei concentration

and the formation of smaller fibrils (~115-nm thickness). PTDPPSe-SiC5 films prepared after filtration exhibited larger fibrillar structures (~200-nm thickness). Without filtration, the PTDPPSe-SiC5 films exhibited similar morphologies but with slightly reduced dimensions (~170-nm thickness) (Figure S3). As-cast TDPPSe-Si copolymer films exhibited smaller fibrillar domains as compared to the annealed films (Figure S4). This implies enhanced charge transport in the annealed films. Large-area AFM scans of solution-sheared TDPPSe-Si films showed highly aligned nanofibrillar networks oriented along the shearing direction (Figure S5). Such aligned molecular networks are known to be highly beneficial to charge transport along the direction of oriented molecular packing.^{10,39}

Grazing incidence X-ray diffraction (GIXD) analyses were also performed to further investigate the crystalline nature and molecular orientation of TDPPSe-based copolymer films. For comparison, thin films of a TDPPSe-based copolymer containing 2-octyldecyl chains (PTDPPSe-ref) were also evaluated. The GIXD images and the corresponding diffractogram profiles of annealed TDPPSe-copolymer films fabricated by drop-casting are shown in Figure 4. The crystallographic parameters are presented in Table S1. Out-of-plane GIXD diffractograms of TDPPSe-Si copolymers exhibited a remarkably strong peak at $q_z = \sim 1.7 \text{ \AA}^{-1}$, regardless of the length of the alkyl spacer in the siloxane-terminated side chains. This implies that the hybrid side chains contribute to the formation of efficient π–π stacking (π-stack distance ~3.6 Å) with face-on orientations.^{40–42} Furthermore, this suggests that these PTDPPSe-Si films would be able to adopt 3-D conduction channels that would enhance charge transport over that of

Table 2. OFET Performance of Optimized TDPPSe-Si Copolymer Films

condition ^a			p-channel			n-channel		
polymer	films	T _a [°C]	μ _{h,max} ^d [cm ² V ⁻¹ s ⁻¹]	μ _{h,avg} ^e [cm ² V ⁻¹ s ⁻¹]	I _{on} /I _{off}	μ _{e,max} [cm ² V ⁻¹ s ⁻¹]	μ _{e,avg} [cm ² V ⁻¹ s ⁻¹]	I _{on} /I _{off}
PTDPPSe-SiC4	spin-coated	N/A ^f	1.38	1.19 (± 0.13) ^g	>10 ⁴	0.79	0.37 (± 0.24)	>10
		220	2.78	1.40 (± 0.56)	>10 ⁵	0.85	0.41 (± 0.29)	>10 ²
	drop-cast	N/A	2.06	1.81 (± 0.17)	>10 ³	0.98	0.45 (± 0.23)	>10
		220	3.72	2.75 (± 0.62)	>10 ⁵	1.13	0.70 (± 0.24)	>10 ²
	solution-sheared	N/A	5.36	5.05 (± 0.31)	>10 ⁴	1.42	1.28 (± 0.15)	>10 ³
		220	6.16	5.12 (± 0.74)	>10 ⁴	3.07	1.39 (± 0.73)	>10 ³
	PTDPPSe-SiC5 ^b	N/A	1.38	1.12 (± 0.26)	>10 ³	0.70	0.40 (± 0.26)	>10
		220	2.92	2.57 (± 0.47)	>10 ⁵	1.13	0.54 (± 0.37)	>10
		N/A	1.82	1.58 (± 0.18)	>10 ⁴	0.78	0.38 (± 0.23)	>10
		220	3.05	2.29 (± 0.47)	>10 ⁴	1.32	0.53 (± 0.40)	>10
PTDPPSe-SiC6 ^c	spin-coated	N/A	4.86	4.58 (± 0.39)	>10 ³	2.06	0.99 (± 0.63)	>10
		220	8.84	5.66 (± 1.45)	>10 ⁴	4.34	1.75 (± 1.49)	>10
	drop-cast	N/A	0.59	0.46 (± 0.15)	>10 ⁴	0.046	0.042 (± 0.003)	>10
		220	1.69	1.54 (± 0.10)	>10 ⁵	0.20	0.14 (± 0.04)	>10 ²
	solution-sheared	N/A	1.07	0.98 (± 0.11)	>10 ⁵	0.095	0.092 (± 0.009)	>10 ³
		220	2.48	2.02 (± 0.38)	>10 ⁵	0.78	0.26 (± 0.24)	>10 ²
	solution-sheared	N/A	3.16	2.87 (± 0.26)	>10 ⁵	0.37	0.18 (± 0.10)	>10 ²
		220	3.97	3.48 (± 0.30)	>10 ⁴	2.20	0.97 (± 0.50)	>10

^aThe p-channel and n-channel characteristics of ambipolar FETs were measured with V_{DS} = -100 and +100 V, respectively. ^bFiltration was applied prior to the solution processing (the FET performance of PTDPPSe-SiC5 films prepared without filtration is included in Table S2). ^cThe performance of PTDPPSe-SiC6 FETs reported in a previous paper³⁴ is included for comparison. ^dThe maximum mobility of the FET devices (L = 50 μm and W = 1000 μm). ^eThe average mobility of the FET devices (L = 50 μm and W = 1000 μm). ^fThermal annealing was not applied. ^gThe standard deviation.

polymer films with only perpendicular π-planes.⁴⁰ In contrast, the annealed film of PTDPPSe-ref did not show any discernible peak in the same range, while the as-prepared film revealed a weak and broad peak centered at $q_z \sim 1.6 \text{ \AA}^{-1}$ (π-stack distance ~3.8 Å). This indicates that the PTDPPSe-ref film completely constitutes edge-on orientations after annealing, while a small portion of the as-prepared film forms face-on orientations. For TDPPSe-Si copolymers, the (100) layer distance decreased with decreasing alkyl spacer length, shifting from 24.6 Å with a hexyl chain to 22.1 Å with a butyl chain. The π-π stacking distance remained relatively constant. This indicates that shorter spacers resulted in the smaller lamellar distance without affecting the π-π stacking distance. Moreover, the TDPPSe-Si copolymer films exhibited higher-order diffraction peaks, revealing relatively long-range order across the film thickness. Interestingly, the crystalline coherence length in the (100) direction increased with increasing length of the spacer in the siloxane-terminated side chains, implying that the hexyl spacer resulted in a higher degree of crystallinity and self-organization. Nevertheless, higher mobilities were observed in TDPPSe-Si copolymer films with alkyl spacers that were shorter than a hexyl group (*vide infra*). This demonstrates the subtle trade-off between enhanced crystallinity, driven by the hydrophobic interactions of the side chain, and the charge transport, hampered by the insulating characteristics of the side chains. As compared to the as-cast films, the annealed polymer films were more crystalline and exhibited denser molecular packing with a lesser (100) layer distance (Figure S6). Furthermore, after thermal treatment, the solution-sheared TDPPSe-Si copolymer films exhibited increased coherence lengths and decreased (100) layer distances. These factors represent the formation of more crystalline and denser molecular structures than those in the drop-cast films (Figures S7 and S8).

Fabrication of Solution-Processed FETs and I-V Characterizations.

To elucidate the relationship between the length of the alkyl spacer in the siloxane side chains and charge transport, bottom-gate top-contact FETs were fabricated using PTDPPSe-SiC4 and PTDPPSe-SiC5. The polymer films (~30-nm thickness) were deposited on OTS-modified SiO₂/Si substrates from a TDPPSe-Si copolymer solution in chlorobenzene (~3 mg mL⁻¹) by spin-coating, drop-casting, or solution-shearing. Solutions of PTDPPSe-SiC4 and PTDPPSe-SiC5 in chlorobenzene were heated to 80 °C to fully dissolve the polymer. Charge transport characteristics were measured in a nitrogen atmosphere. The experimental details regarding surface modification^{43–45} and FET fabrication are included in the Supporting Information. The performance of FETs fabricated with PTDPPSe-SiC4 and PTDPPSe-SiC5 is summarized in Table 2. The TDPPSe-Si copolymer exhibited ambipolar characteristics regardless of the type or length of side chain, as predicted by DFT calculations on the TDPP-selenophene copolymer.³⁴ The relatively lower on/off ratios were observed from n-channel operation, due to the high off-current engendered by the superior hole conduction. The electrical performance of the solution-sheared polymer thin films was superior to that of the other solution-processed films due to the highly crystalline and aligned nature of the solution-sheared films, as observed in XRD and AFM analyses. Furthermore, the TDPP-selenophene copolymers containing siloxane-terminated side chains were easy to deposit as thin films on highly hydrophobic surfaces such as crystalline OTS-modified SiO₂/Si substrates. Very low contact angles were observed when the polymer solution was placed on these hydrophobic substrates, indicating that the siloxane-containing copolymers tended to have lower surface tensions than the same copolymers with conventional alkyl chains. This resulted in good wettability and facilitated the formation of uniform thin films. Figure 5 shows the representative transfer and output

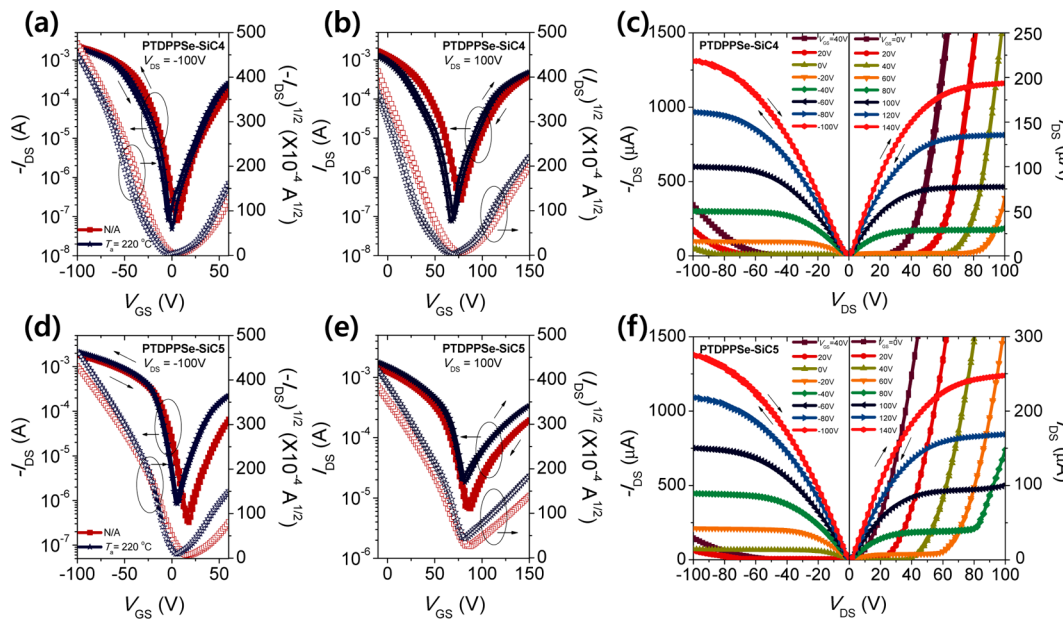


Figure 5. Current–voltage (I – V) characteristics of OFETs with optimized thin-film fabricated by solution-shearing method. Transfer characteristics for PTDPPSe-SiC4 films of as-cast and annealed at 220 °C at (a) hole-, (b) electron-enhancement operation with $V_{DS} = -100$ and +100 V, respectively. (c) Output characteristics for PTDPPSe-SiC4 films after annealing at 220 °C. Transfer characteristics for PTDPPSe-SiC5 films of as-cast and annealed at 220 °C at (d) hole-, (e) electron-enhancement operation with $V_{DS} = -100$ and +100 V, respectively. (f) Output characteristics for PTDPPSe-SiC5 films after annealing at 220 °C ($L = 50 \mu\text{m}$ and $W = 1000 \mu\text{m}$).

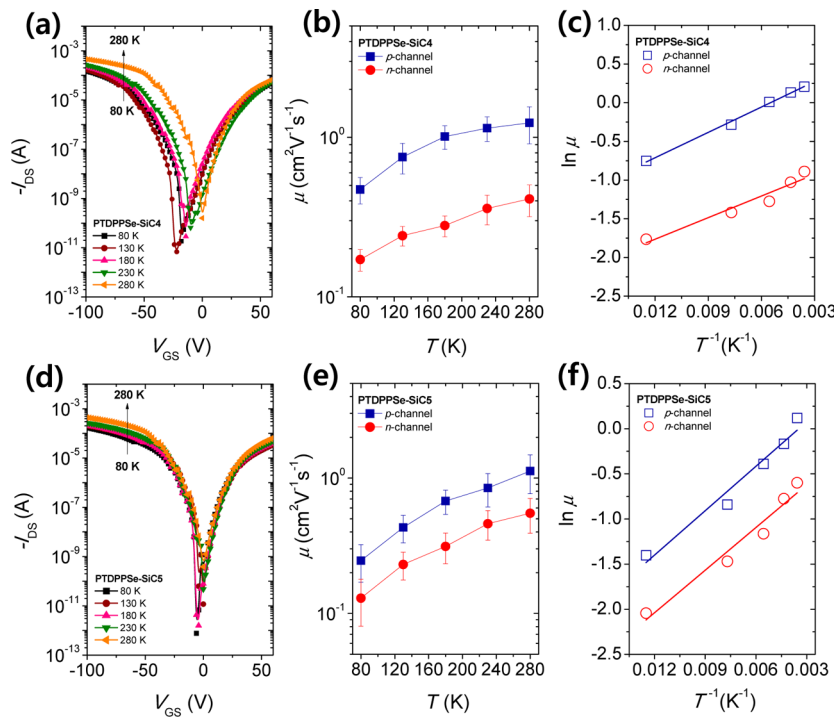


Figure 6. Temperature effects on the electrical characteristics of drop-cast TDPPSe-Si copolymer FETs. (a)–(c) PTDPPSe-SiC4 FETs. (a) I_{DS} – V_G characteristics at various temperatures (80–280 K) with $V_{DS} = -100$ V. (b) Temperature dependence of electron and hole mobilities in vacuum. (c) Arrhenius plot of the temperature dependence of the FET mobilities. The linear fits to the Arrhenius plot revealed E_A 's of 9 meV for p-channel and 8 meV for n-channel operation. (d)–(f) PTDPPSe-SiC5 FETs. (d) I_{DS} – V_G characteristics at various temperatures (80–280 K) with $V_{DS} = -100$ V. (e) Temperature dependence of electron and hole mobilities in vacuum. (f) Arrhenius plot of the temperature dependence of the FET mobilities. The linear fits to the Arrhenius plot revealed E_A 's of 14 meV for both p-channel and n-channel operations. A slight decrease in the average ambipolar mobility is presumably due to the exposure of devices to ambient air during the transfer process from a N_2 -filled glovebox to the vacuum chamber.

characteristics of optimized FETs based on solution-sheared films of PTDPPSe-SiC4 and PTDPPSe-SiC5. Both polymers exhibited typical V-shaped, ambipolar behavior. Hysteresis was

negligible in both the transfer and the output characteristics of PTDPPSe-SiC4 and PTDPPSe-SiC5 FETs. PTDPPSe-SiC4 films obtained from the as-prepared solutions without filtration

also showed excellent electrical performance. The as-cast, solution-sheared **PTDPPSe-SiC4** films showed remarkably high hole and electron mobilities of up to 5.36 and $1.42 \text{ cm}^2 \text{ V}^{-1} \text{ s}^{-1}$, respectively. These mobilities are approximately 2 and 3 times higher than those measured on the other solution-processed films. Even higher hole and electron mobilities of 6.16 and $3.07 \text{ cm}^2 \text{ V}^{-1} \text{ s}^{-1}$ were obtained after annealing these films at 220°C , which demonstrated the effect of thermal annealing on charge transport. Similarly, very high charge carrier mobilities were obtained in annealed **PTDPPSe-SiC5** films ($\mu_h = 5.97 \text{ cm}^2 \text{ V}^{-1} \text{ s}^{-1}$ and $\mu_e = 3.94 \text{ cm}^2 \text{ V}^{-1} \text{ s}^{-1}$) without prior solution filtration (Table S2). These mobilities are higher than those of previously reported **PTDPPSe-SiC6** films. Note that under identical conditions, **PTDPPSe-SiC4** exhibited the highest average mobilities due to the formation of optimized microstructures that facilitated charge transport. This result is consistent with the relatively dense molecular packing observed in XRD analyses of the **PTDPPSe-SiC4** films. However, when solutions of **PTDPPSe-SiC5** were passed through a syringe filter prior to solution-shearing, the annealed films exhibited extraordinary hole and electron mobilities of up to 8.84 and $4.34 \text{ cm}^2 \text{ V}^{-1} \text{ s}^{-1}$, respectively. This is in line with the formation of larger nanofibrillar crystalline domains after filtration. To our knowledge, these hole and electron mobilities are the highest reported ambipolar mobilities measured in organic or polymer-based semiconductors to date. These results demonstrate that charge transport is critically affected by both solubility and processing architecture. Achieving the desired results is a balancing act between these two factors. In particular, optimization of solution processing parameters to facilitate the formation of homogeneous films is important for device fabrication using polymer semiconductors with short side chains. The hole-dominant transport characteristics are presumably due to smaller injection barriers for holes with respect to the gold contacts. For the TDPPSe-Si copolymers, the HOMO–LUMO energy levels gradually shifted depending on the side-chain length. The lowest HOMO level was observed in **PTDPPSe-SiC4**.

The charge transport behavior of the TDPPSe-Si copolymers and their temperature dependencies were investigated between 80 and 280°K at 1×10^{-5} Torr. The measurements were conducted with a temperature step of 50 K and a time delay of 1 h for stabilization. The hole and electron mobilities of the **PTDPPSe-SiC4** and **PTDPPSe-SiC5** FETs increased with increasing temperature, yielding a positive mobility temperature coefficient ($d\mu/dt > 0$) (Figure 6). These results indicate that the **PTDPPSe-SiC4** and **PTDPPSe-SiC5** FETs follow a thermally activated charge hopping transport model.⁴⁶ Furthermore, Arrhenius plots of temperature-dependent mobility in *p*- and *n*-channel operations were generated for each copolymer to estimate the activation energy (E_A) (Figure 6). For **PTDPPSe-SiC4** FETs, linear fits of the data revealed E_A 's of 9 and 8 meV for *p*- and *n*-channel operations, respectively. **PTDPPSe-SiC5** FETs yielded E_A 's of 14 meV for both *p*- and *n*-channel operations. These E_A 's are lower than those of high-performance D–A copolymers with alkyl chains.¹¹

The complementary metal–oxide–semiconductor (CMOS)-like inverter characteristics of TDPPSe-Si copolymers were also investigated using two ambipolar transistors. Output voltage (V_{OUT}) was monitored as a function of input voltage (V_{IN}) at a constant supply bias (V_{DD}). The voltage transfer characteristic (VTC) curves and corresponding output voltage gains of

PTDPPSe-SiC4 and **PTDPPSe-SiC5** are shown in Figure S9. High gains of 55.1 and 53.0 were obtained from **PTDPPSe-SiC4** and **PTDPPSe-SiC5**, respectively, although asymmetry in mobilities and threshold voltages in *p*- and *n*-channel operation resulted in a hysteresis between the forward and reverse sweeps and a signal inversion at a relatively large V_{IN} .

CONCLUSION

Solution-processable, high-performance, ambipolar polymer semiconductors were developed via side-chain engineering of TDPP-selenophene copolymers with well-delocalized HOMO and LUMO isosurfaces over the polymer backbone (**PTDPPSe-SiC_n**, where $n = 4–6$). The length of the alkyl spacer group in the hybrid side chain was delicately tuned to induce denser molecular packing and facilitate charge transport through 3-D conduction channels. Although both crystallinity and solubility were enhanced with increasing alkyl spacer length, the shorter side chains induced smaller lamellar spacing while retaining a close $\pi-\pi$ stacking distance, leading to enhanced charge transport in the as-prepared films. **PTDPPSe-SiC5** films prepared in optimized conditions exhibited the best electrical performance with unprecedentedly high hole and electron mobilities of 8.84 and $4.34 \text{ cm}^2 \text{ V}^{-1} \text{ s}^{-1}$, respectively. Our results demonstrate the subtle trade-off between crystallinity, which is enhanced by the insulating side chains, and the charge transport. In addition, our findings provide new insight into the molecular design of organic electronics. Several remarkable features, including high mobility, good wettability on hydrophobic surfaces, and low activation energies for charge hopping, make these polymers highly promising materials for use in printed and flexible electronics.

ASSOCIATED CONTENT

Supporting Information

General synthetic procedures, experimental section, characterization of all of the intermediates, and additional figures (cyclic voltammetry plots, UPS spectroscopy, additional AFM and GIXD images, and complementary-like inverter characteristics). This material is available free of charge via the Internet at <http://pubs.acs.org>.

AUTHOR INFORMATION

Corresponding Author

joonhoh@unist.ac.kr; yang@unist.ac.kr

Author Contributions

[†]These authors contributed equally.

Notes

The authors declare no competing financial interest.

ACKNOWLEDGMENTS

This work was supported by the National Research Foundation of Korea (NRF) funded by the Korean Government (MEST) (Grant nos. 2010-0019408, 2010-0026916, 2010-0025292, 2011-0017174, 2013R1A1A1A05004475), Global Frontier Research Center for Advanced Soft Electronics (Grant no.: 2011-0031628), and the International Cooperation of the Korea Institute of Energy Technology Evaluation and Planning (KETEP) grant funded by the Korea government Ministry of Knowledge Economy (2012T100100740).

■ REFERENCES

- (1) Yan, H.; Chen, Z.; Zheng, Y.; Newman, C.; Quinn, J. R.; Dotz, F.; Kastler, M.; Facchetti, A. *Nature* **2009**, *457*, 679.
- (2) McCulloch, I.; Heeney, M.; Bailey, C.; Genevicius, K.; MacDonald, I.; Shkunov, M.; Sparrowe, D.; Tierney, S.; Wagner, R.; Zhang, W.; Chabinyc, M. L.; Kline, R. J.; McGehee, M. D.; Toney, M. F. *Nat. Mater.* **2006**, *5*, 328.
- (3) Gelinck, G. H.; Huitema, H. E. A.; van Veenendaal, E.; Cantatore, E.; Schrijnemakers, L.; van der Putten, J. B. P. H.; Geuns, T. C. T.; Beenhakkers, M.; Giesbers, J. B.; Huisman, B.-H.; Meijer, E. J.; Benito, E. M.; Touwslager, F. J.; Marsman, A. W.; van Rens, B. J. E.; de Leeuw, D. M. *Nat. Mater.* **2004**, *3*, 106.
- (4) Rogers, J. A.; Bao, Z.; Baldwin, K.; Dodabalapur, A.; Crone, B.; Raju, V. R.; Kuck, V.; Katz, H.; Amundson, K.; Ewing, J.; Drzaic, P. *Proc. Natl. Acad. Sci. U.S.A.* **2001**, *98*, 4835.
- (5) Subramanian, V.; Chang, P. C.; Lee, J. B.; Molesa, S. E.; Volkman, S. K. *IEEE Trans. Compon. Packag. Technol.* **2005**, *28*, 742.
- (6) Someya, T.; Kato, Y.; Sekitani, T.; Iba, S.; Noguchi, Y.; Murase, Y.; Kawaguchi, H.; Sakurai, T. *Proc. Natl. Acad. Sci. U.S.A.* **2005**, *102*, 12321.
- (7) Lu, G.; Usta, H.; Risko, C.; Wang, L.; Facchetti, A.; Ratner, M. A.; Marks, T. J. *J. Am. Chem. Soc.* **2008**, *130*, 7670.
- (8) Chua, L.-L.; Zaumseil, J.; Chang, J.-F.; Ou, E. C. W.; Ho, P. K. H.; Sirringhaus, H.; Friend, R. H. *Nature* **2005**, *434*, 194.
- (9) Noh, Y.-Y.; Zhao, N.; Caironi, M.; Sirringhaus, H. *Nat. Nanotechnol.* **2007**, *2*, 784.
- (10) Giri, G.; Verploegen, E.; Mannsfeld, S. C. B.; Atahan-Evrenk, S.; Kim, D. H.; Lee, S. Y.; Becerril, H. A.; Aspuru-Guzik, A.; Toney, M. F.; Bao, Z. *Nature* **2011**, *480*, 504.
- (11) Li, J.; Zhao, Y.; Tan, H. S.; Guo, Y. L.; Di, C. A.; Yu, G.; Liu, Y. Q.; Lin, M.; Lim, S. H.; Zhou, Y. H.; Su, H. B.; Ong, B. S. *Sci. Rep.* **2012**, *2*, 754.
- (12) Capelli, R.; Toffanin, S.; Generali, G.; Usta, H.; Facchetti, A.; Muccini, M. *Nat. Mater.* **2010**, *9*, 496.
- (13) Meijer, E. J.; de Leeuw, D. M.; Setayesh, S.; van Veenendaal, E.; Huisman, B. H.; Blom, P. W. M.; Hummelen, J. C.; Scherf, U.; Klapwijk, T. M. *Nat. Mater.* **2003**, *2*, 678.
- (14) Dodabalapur, A.; Katz, H. E.; Torsi, L.; Haddon, R. C. *Science* **1995**, *269*, 1560.
- (15) Chen, Z.; Lemke, H.; Albert-Seifried, S.; Caironi, M.; Nielsen, M. M.; Heeney, M.; Zhang, W.; McCulloch, I.; Sirringhaus, H. *Adv. Mater.* **2010**, *22*, 2371.
- (16) Klauk, H.; Zschieschang, U.; Pflaum, J.; Halik, M. *Nature* **2007**, *445*, 745.
- (17) Zaumseil, J.; Friend, R. H.; Sirringhaus, H. *Nat. Mater.* **2006**, *5*, 69.
- (18) Bürgi, L.; Turbiez, M.; Pfeiffer, R.; Bienewald, F.; Kirner, H.-J.; Winniewisser, C. *Adv. Mater.* **2008**, *20*, 2217.
- (19) Sonar, P.; Singh, S. P.; Li, Y.; Soh, M. S.; Dodabalapur, A. *Adv. Mater.* **2010**, *22*, 5409.
- (20) Chen, Z.; Lee, M. J.; Shahid Ashraf, R.; Gu, Y.; Albert-Seifried, S.; Meedom Nielsen, M.; Schroeder, B.; Anthopoulos, T. D.; Heeney, M.; McCulloch, I.; Sirringhaus, H. *Adv. Mater.* **2012**, *24*, 647.
- (21) Yuen, J. D.; Fan, J.; Seifter, J.; Lim, B.; Hufschmid, R.; Heeger, A. J.; Wudl, F. *J. Am. Chem. Soc.* **2011**, *133*, 20799.
- (22) Thompson, B. C.; Fréchet, J. M. J. *Angew. Chem., Int. Ed.* **2008**, *47*, 58.
- (23) Gsänger, M.; Oh, J. H.; Könemann, M.; Höffken, H. W.; Krause, A.-M.; Bao, Z.; Würthner, F. *Angew. Chem., Int. Ed.* **2010**, *49*, 740.
- (24) Lei, T.; Cao, Y.; Fan, Y.; Liu, C.-J.; Yuan, S.-C.; Pei, J. *J. Am. Chem. Soc.* **2011**, *133*, 6099.
- (25) Osaka, I.; Zhang, R.; Sauvé, G. v.; Smilgies, D.-M.; Kowalewski, T.; McCullough, R. D. *J. Am. Chem. Soc.* **2009**, *131*, 2521.
- (26) Sung, A.; Ling, M. M.; Tang, M. L.; Bao, Z.; Locklin, J. *Chem. Mater.* **2007**, *19*, 2342.
- (27) Mondal, R.; Ko, S.; Verploegen, E.; Becerril, H. A.; Toney, M. F.; Bao, Z. *J. Mater. Chem.* **2011**, *21*, 1537.
- (28) Bao, Z.; Lovinger, A. J. *Chem. Mater.* **1999**, *11*, 2607.
- (29) Li, H.; Mei, J.; Ayzner, A. L.; Toney, M. F.; Tok, J. B. H.; Bao, Z. *Org. Electron.* **2012**, *13*, 2450.
- (30) Tuladhar, S. M.; Sims, M.; Choulis, S. A.; Nielsen, C. B.; George, W. N.; Steinke, J. H. G.; Bradley, D. D. C.; Nelson, J. *Org. Electron.* **2009**, *10*, 562.
- (31) Kline, R. J.; DeLongchamp, D. M.; Fischer, D. A.; Lin, E. K.; Richter, L. J.; Chabinyc, M. L.; Toney, M. F.; Heeney, M.; McCulloch, I. *Macromolecules* **2007**, *40*, 7960.
- (32) Torsi, L.; Farinola, G. M.; Marinelli, F.; Tanese, M. C.; Omar, O. H.; Valli, L.; Babudri, F.; Palmisano, F.; Zambonin, P. G.; Naso, F. *Nat. Mater.* **2008**, *7*, 412.
- (33) Mei, J.; Kim, D. H.; Ayzner, A. L.; Toney, M. F.; Bao, Z. *J. Am. Chem. Soc.* **2011**, *133*, 20130.
- (34) Lee, J.; Han, A.-R.; Kim, J.; Kim, Y.; Oh, J. H.; Yang, C. *J. Am. Chem. Soc.* **2012**, *134*, 20713.
- (35) Lei, T.; Dou, J.-H.; Pei, J. *Adv. Mater.* **2012**, *24*, 6457.
- (36) Zhang, F.; Hu, Y.; Schuettfert, T.; Di, C.-a.; Gao, X.; McNeill, C. R.; Thomsen, L.; Mannsfeld, S. C. B.; Yuan, W.; Sirringhaus, H.; Zhu, D. *J. Am. Chem. Soc.* **2013**, *135*, 2338.
- (37) Sariciftci, N. S. *Primary Photoexcitations in Conjugated Polymers: Molecular Exciton versus Semiconductor Band Model*; World Scientific: Singapore, 1997.
- (38) Zhu, Y.; Champion, R. D.; Jenekhe, S. A. *Macromolecules* **2006**, *39*, 8712.
- (39) Becerril, H. A.; Roberts, M. E.; Liu, Z.; Locklin, J.; Bao, Z. *Adv. Mater.* **2008**, *20*, 2588.
- (40) Rivnay, J.; Steyrleuthner, R.; Jimison, L. H.; Casadei, A.; Chen, Z.; Toney, M. F.; Facchetti, A.; Neher, D.; Salleo, A. *Macromolecules* **2011**, *44*, 5246.
- (41) Zhang, X.; Richter, L. J.; DeLongchamp, D. M.; Kline, R. J.; Hammond, M. R.; McCulloch, I.; Heeney, M.; Ashraf, R. S.; Smith, J. N.; Anthopoulos, T. D.; Schroeder, B.; Geerts, Y. H.; Fischer, D. A.; Toney, M. F. *J. Am. Chem. Soc.* **2011**, *133*, 15073.
- (42) Jimison, L. H.; Toney, M. F.; McCulloch, I.; Heeney, M.; Salleo, A. *Adv. Mater.* **2009**, *21*, 1568.
- (43) Ito, Y.; Virkar, A. A.; Mannsfeld, S.; Oh, J. H.; Toney, M.; Locklin, J.; Bao, Z. *J. Am. Chem. Soc.* **2009**, *131*, 9396.
- (44) Schmidt, R.; Oh, J. H.; Sun, Y.-S.; Deppisch, M.; Krause, A.-M.; Radacki, K.; Braunschweig, H.; Könemann, M.; Erk, P.; Bao, Z.; Würthner, F. *J. Am. Chem. Soc.* **2009**, *131*, 6215.
- (45) Virkar, A.; Mannsfeld, S.; Oh, J. H.; Toney, M. F.; Tan, Y. H.; Liu, G. Y.; Scott, J. C.; Miller, R.; Bao, Z. *Adv. Funct. Mater.* **2009**, *19*, 1962.
- (46) Coropceanu, V.; Cornil, J.; da Silva Filho, D. A.; Olivier, Y.; Silbey, R.; Brédas, J.-L. *Chem. Rev.* **2007**, *107*, 926.